Horizontal exchange across the thermal bar front: laboratory and numerical modelling

Natalia Demchenko and Irina Chubarenko

ABSTRACT

Laboratory and numerical experiments have revealed physical reasons for the permeability of the thermal bar to horizontal transport. The thermal bar is understood as a front associated with the temperature of maximum density ($T_m = 3.98\ ^\circ$C for fresh water). Laboratory experiments were performed in a 2-metre-long non-rotating channel with a sloping bottom, filled with water with $T < T_m$ and naturally heated from above. Analysis of Particle Image Velocimetry (PIV) images revealed water dynamics in the presence of T_m. It was revealed that the compensating flow in intermediate layers is responsible for the horizontal exchange across the thermal bar front. We applied a 3D non-hydrostatic MIKE3-FlowModel (www.dhi.dk) to investigate the permeability of the spring thermal bar in basins on the scale of lakes and a laboratory flume. We performed an analysis of the concentration distribution of 12 passive tracers released at different locations in the flow domain. Scaling analysis, corroborated by the results of laboratory and numerical experiments, predicts the discharge across the thermal bar as $Q = 0.1[g \times \Delta\rho/\rho_0]^{1/2} h^{3/2}$, where h is the depth of the upper thermo-active layer, ρ_0 is a maximum density and $\Delta\rho$ is a characteristic horizontal density difference. A combined analysis of data shows that this law is obeyed.

Key words | buoyancy flux, flow-rate, horizontal exchange, onshore flow, passive tracers, thermal bar

Natalia Demchenko (corresponding author)
Irina Chubarenko
P.P. Shirshov Institute of Oceanology RAS,
Atlantic Branch,
Prospect Mira 1, 236022,
Kaliningrad,
Russia
E-mail: *nata_dem@yahoo.com*;
ndemchenko@mail.ru

INTRODUCTION

The 'thermal bar' is a remarkable phenomenon, seasonally arising at mid-latitudes in large lakes and in coastal regions, when the water temperature gradually increases in spring (or decreases in autumn) and crosses the temperature of maximum density (hereafter referred to as T_m; for fresh water, $T_m \approx 3.98\ ^\circ$C). In late autumn, a gradual transition from $T > T_m$ to $T < T_m$ is driven by seasonal cooling, while the inverse process takes place under spring warming. In both cases, shallow waters respond faster to the external thermal forcing, so water with a temperature of $T = T_m$ appears first in the shallowest regions. The T_m isotherm is initially aligned with the shoreline. During the time of heating/cooling it advances offshore and becomes generally aligned with the isobaths. The thermal expansion coefficient of water, $\alpha = 1/\rho(\partial\rho/\partial T)$, changes sign at $T = T_m$. Therefore, the response of a water column to the same external heat flux is principally different on either side of T_m: on one side of the T_m-isotherm (the shallower side) the water column becomes increasingly stably stratified; while on the other side (the deeper side), vertical mixing by thermo-gravitational convection takes place (Chubarenko *et al.* 2008). Thus, the location of the T_m-isotherm at the water surface indicates the border between water masses with different mixing characteristics under the same external conditions (Rodgers 1966; Tikhomirov 1982). For simplicity, we shall expand further on the conditions of the 'spring' thermal bar. As spring commences, the water begins to warm up, vertical convection homogenises water columns, which involves vertical mixing of different water masses at different depths; thus, water temperature becomes dependent on depth and T_m is reached in shallow nearshore regions first and only later in the deeper areas.

doi: 10.2166/wqrjc.2012.037

F. A. Forel (1901), who offered an explanation for it, observed this phenomenon first in Lake Geneva. Following those first observations and explanations, the formation of the thermal bar front has been attributed to the cabbelling process. This is a process where parcels of surface water at the T_m-isotherm (which is generally parallel to the shore and isobaths) begin to sink, because they are denser than the water to either side. The sinking water is replaced by water parcels from opposite sides of the bar with temperatures slightly above and slightly below T_m; these get mixed, generating a water mass of temperature T_m, and so the process continues (see, e.g., Tikhomirov 1982). Obviously, under this hypothesis, the thermal bar restricts horizontal exchange and intensifies vertical mixing (Elliot & Elliot 1970; Tikhomirov 1982; Kreiman 1989).

However, field data from Lake Ladoga (Rymiantsev & Drabkova 2002) have demonstrated that the thermal bar front is not a type of vertical wall; rather, it is a 3D surface with a very small angle of inclination of the frontal division (about 0.001), i.e., warm stratified waters overlying colder quasi-isothermal waters. Rymiantsev & Drabkova (2002) identified that sometimes water with characteristics of the warm stratified part was observed within the cold quasi-isothermal region; thus demonstrating that water exchange between the stably and unstably stratified parts does exist and that the frontal zone is not an impermeable barrier between the shallow and deeper parts of the lake.

Rao *et al.* (2004) investigated the spring thermal bar circulation in Lake Ontario using a vertical chain of thermistors and current meters. One interesting observation from this field experiment is that at the beginning of the thermal bar process, at a water depth of 20 m, the 3.98 °C-isotherm first appeared but that the water became slightly cooler (~3.5 °C) during the next 3 days; then the thermal bar reappeared and was present at this location for a couple of days more. The authors suggested that the influence of moderate westerly winds could account for this through onshore transport from deeper waters. From that moment on, the 3.98 °C-isotherm was more or less stationary at this location for the next 2 weeks; however, cross-shore currents flowed in the offshore direction near the thermal bar region.

Observed mean cross-shore velocities vary significantly from the thermal bar to the pre- and post-thermal bar seasons. The onshore flow towards the bottom, during the pre-thermal bar period, was larger than during the post-thermal bar period. Surface currents on the nearshore side of the thermal bar are directed towards the thermal bar, which indicates the strong possibility of offshore horizontal heat transport from nearshore areas in the surface layer, during the pre-thermal bar and thermal bar period. The mean alongshore currents did not change direction during the thermal bar period; however, the mean cross-shore velocities showed offshore flow during the thermal bar period.

During thermal bar presence, the mean cross-shore flow was reduced, although it appeared that the exchange is depth dependent. The magnitude of both alongshore and cross-shore exchange coefficients decreased when the thermal bar was within mid-depth (<40 m). In contrast to an earlier study (Gbah & Murthy 1998), from mid-depth onward, the thermal bar did not show an effect on alongshore exchange coefficients, but cross-shore exchanges decreased marginally. The authors concluded that the thermal bar plays an important role in suppressing horizontal mixing in the shallows but that its effect is not that significant in deeper offshore areas. The lateral current shear between the nearshore and the thermal bar region could be an important factor in maintaining horizontal exchange in deeper waters (Rao *et al.* 2004).

Many laboratory observations concerning horizontal convection driven by heating/cooling through opposite halves of the horizontal base or above the slope have reproduced the specific features of thermal and current fields, either on the cold or warm side of the thermal bar front (Imberger 1974; Patterson & Imberger 1980; Bejan *et al.* 1981). However, all these experimentalists used a viscous velocity scale. Elliot (1970) developed a model for the circulation associated with the thermal bar, by assuming a balance between vertical shear and the horizontal pressure gradient. However, the spin-up time-scale, based on the depth of the experimental tank and molecular values for viscosity, suggests that a viscous/buoyancy balance would not be achieved in the entire tank before the experiment ended and that inertial effects, particularly in the deeper parts of the tank, could be important. Farrow (1995a) has presented an asymptotic solution (based on small bottom slope) for an idealised model for the thermal bar phenomenon, in a non-rotating frame that included inertial effects.

It was established that in the viscous regime (in the shallows), the velocity is essentially modulated by the sign and magnitude of the pressure gradient, while in the deeper waters, the inertia of the existing flow plays a role in the dynamics. Malm *et al.* (1993) showed that the thermal bar moves into the deep part more rapidly than a viscous balance can occur; thus, unsteady inertial effects could be important in determining the overall circulation pattern.

Farrow (1995b) developed a numerical model exposing a number of remarkable features of the thermal bar: (1) the existence of an offshore subsurface jet and a downslope current, with an onshore flow in between, appearing at different stages of the thermal bar development and (2) both the initial 'slow' phase and the later 'fast' phase of the thermal bar propagation.

Ivey & Hamblin (1989), in their laboratory experiments on convection of water close to the density maximum, revealed that the form of the velocity profile changes to one with jet-like flows when $\mathrm{Ra} > \mathrm{Pr}^4 A^{-4}$ (Rayleigh number, $\mathrm{Ra} = g\alpha(\Delta T)^2 h^3/\nu k$, aspect ratio of cavity, $A = h/l$, Prandtl number, $\mathrm{Pr} = \nu/k$, where g is gravitational constant, α is nonlinear coefficient of thermal expansion, ΔT is 1/2 the difference in endwall jacket temperatures, h is height of the cavity, l is length of the half cavity, ν is kinematic viscosity, k is thermal diffusivity). It was also shown that beyond the critical depth the flow became unstable and underwent a series of large-scale horizontal meanders while sinking. Hence, the frontal region no longer acted as a barrier to horizontal transport.

Despite all the investigations, some questions remain unanswered. The point addressed in the present study is to show that the compensating onshore flow in the intermediate layers provides the horizontal transport across the T_m-isotherm.

METHODS

Experimental set-up

The experiments were performed in a 2-metre-long water channel with a sloping bottom; the slope being defined by the aspect ratio of the maximum water depth H to the tank length L, with $A = H/L \approx 0.1$ (see Figure 1). The tank contained tap water cooled to a temperature of 1 °C by a cooling machine (ULTRA KRYOMAT TK-30D) and melting

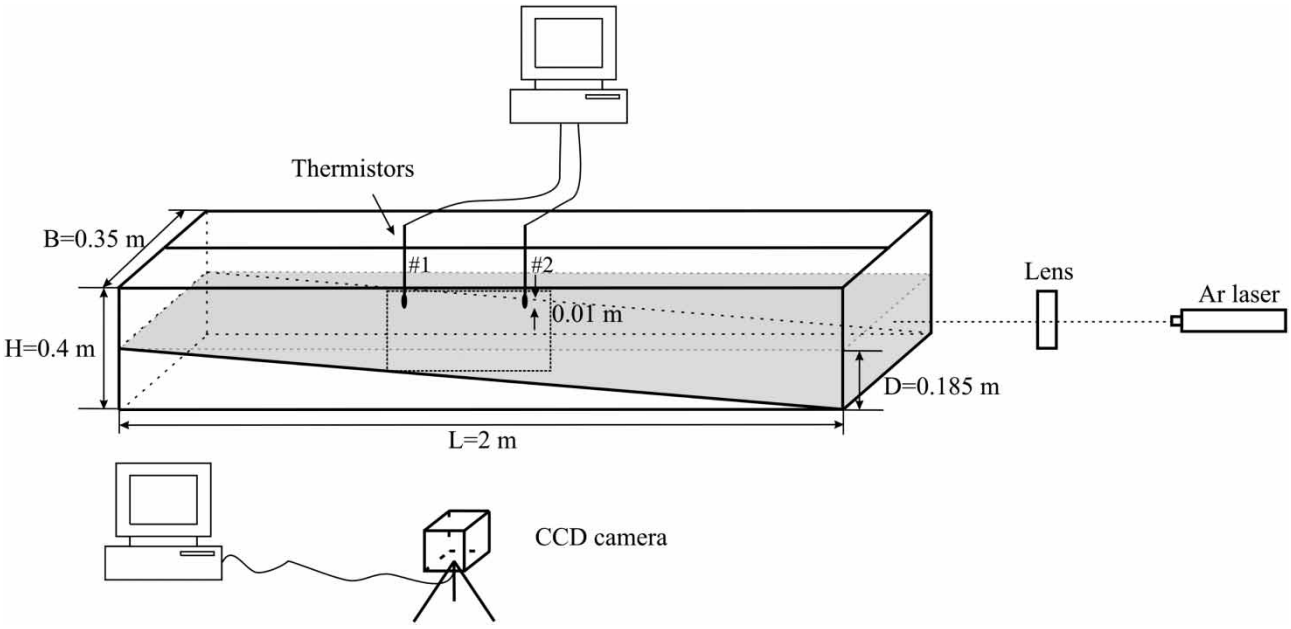

Figure 1 | Sketch of the experimental set-up. Grey shading indicates the water body above the inclined bottom with the maximum depth $H = 0.185$ m. The bottom inclination is given by the aspect ratio, $A = H/L \sim 0.1$, with $L = 2$ m the total length of the tank. Two calibrated thermistors are placed at a depth of 1 cm along the central axis of the flume at positions $x = 0.74$ and 0.98 m, corresponding to local depths of 0.074 and 0.098 m. The vertical size of the sensing element of each thermistor is about 3–7 mm. Dashed square indicates region of illumination where Pliolite particles were seeded.

ice cubes on the free surface. Subsequently, the water temperature gradually increased due to heat-exchange through the free surface with the warmer ambient air ($T_{air} \sim 22\ ^{\circ}C$). Estimates were made of the value of the total heat flux through the free surface due to convective and latent heat fluxes, based on the change in basin heat content over time. A portable thermistor placed in the deep part of the basin during the experiment measured vertical temperature profiles to define the temperature values in the well-mixed core. Using the formula for the heat content of the basin:

$$F \cdot S \cdot t = c_p \cdot \rho \cdot V \cdot (T_2 - T_1)$$

(where F is total heat flux, S is surface area of a basin, t is duration of the experiment, c_p is thermal conductivity, ρ is reference density, V is volume of the basin, T_2 and T_1 are temperatures of well-mixed core at the beginning and at the end of the experiment, respectively) we estimated values of the total heat flux that were approximately 100–300 W/m^2 in the different experiments. This implies a buoyancy flux through the surface in a range from approximately -5×10^{-9} m^2/s^3 (destabilising buoyancy flux, when $2.35\ ^{\circ}C < T < 3.98\ ^{\circ}C$) to $+1.4 \times 10^{-8}$ m^2/s^3 (stabilising buoyancy flux, when $3.9\ ^{\circ}C < T < 9.2\ ^{\circ}C$), depending on the water temperature. Insulating material thermally protected the sidewalls and the bottom of the tank.

The subsurface temperature in the window was monitored by two calibrated thermistors (AD590 type, One Technology Way, Norwood, MA, USA) along the centreline at $x = 0.74$, 0.98 m placed in the 1-cm surface layer. The length of the sensing element of each thermistor was about 3–7 mm; the sampling frequency of these thermistors was 1/30 s. According to the specifications provided by the manufacturer, the accuracy of the thermistors is 0.001 °C.

For the optical flow measurement, we used only the middle part of the tank (64–114 cm from the beginning of the slope). Pliolite particles were initially sieved to have maximum diameters of 250 μm, soaked in the water and injected into the fluid in the tank, in specific areas of study. These particles were illuminated by an argon ion laser, which was refracted by two negative lenses. The motion of the particles was recorded by an Adimec camera MX12P with a 50-mm lens (taking 14 images every 5 min during the experiment). We used DigiFlow software (see www.dalzielresearch.com) to track the particles and calculate the velocity fields.

Experimental results of the flow rates, which were obtained in a 5-metre-long basin with a sloping bottom, during the 'spring' thermal bar by Chubarenko *et al.* (2008), are used in this paper (see Table 1). Photographing tracks from potassium permanganate crystals ($KMnO_4$) dropped into the tank to produce vertical dyelines permitted investigation of the flow structure. The photo recording was processed using CorelDRAW in order to obtain velocity profiles. Two images of the same size with an appropriate time step were selected and their centres vertically aligned using CorelDRAW. The surface and bottom were defined on the pictures and dyelines were outlined using the Bezier tool. The two profiles were combined with each other and the coordinate in each mesh for each profile defined. Then, the mesh size was recalculated (in metres) using the ruler scale (there is a ruler on each picture) and the depth of the profile location was defined. The x-coordinate of one profile was subtracted from the x-coordinate of the other and the difference was multiplied by the mesh size (in metres) in order to estimate the horizontal displacement.

Table 1 | Laboratory and numerical data used in Figure 8

Type of data	Q [m^2/s]	h [m]	$\Delta\rho/\rho_0$ [kg/m^3]
Chubarenko *et al.* (2008)	7.1×10^{-7}	0.3	0.000017
	1.46×10^{-6}	0.3	0.000027
	3.8×10^{-6}	0.4	0.00004
	1.7×10^{-6}	0.4	0.000056
	5.5×10^{-6}	0.6	0.000067
Numerical modelling:			
Scale of flume	4.9×10^{-5}	0.055	0.00018
	7.14×10^{-5}	0.08	0.00017
	8.9×10^{-5}	0.1	0.00018
	6.8×10^{-5}	0.13	0.00021
	5.1×10^{-5}	0.15	0.00022
Scale of lake	9×10^{-3}	5	0.000022
	1.6×10^{-2}	7	0.000023
	2.8×10^{-2}	11	0.00003
	2.6×10^{-2}	18	0.00005
	7.4×10^{-2}	22	0.000067
	8×10^{-2}	24	0.00009

Finally, in order to estimate a velocity value for each layer, the displacement was divided by the time period between the two images. Then, these velocity profiles were recalculated into flow rates as follows: the average velocity for each vertical layer was multiplied by the thickness of this layer over the whole depth. The values of flow rates were chosen only for positive flows over the entire water depth, as calculated in the numerical model.

Numerical model

Numerical modelling of the spring thermal bar was performed using a 3D non-hydrostatic MIKE3-FlowModel (DHI Water & Environment, http://www.dhi.dk/) on the scale of the laboratory flume and lake. One of the simulated flow domains was close to the laboratory configuration (see Figure 1): 20 cm maximum depth; 80 cm width; 320 cm total length with the sloping bottom extending over a length of 200 cm. As in the experiments, the bottom slope, defined by the aspect ratio of the maximum water depth H to the slope length L, was taken to be $A = H/L \sim 0.1$. In order to check the accuracy of the simulation results we applied grid refinement. In order to obtain the component of horizontal velocity u more precisely, we used two different mesh sizes: (a) 80×20 cells (i.e., with mesh size 0.04 m) and (b) 320×80 cells (with mesh size 0.01 m) in the horizontal and 20 layers (at 1-cm intervals) in the vertical. The integration time step was 0.03 s for grid (a) and 0.01 s for grid (b). No wind stress was applied and the surface heating was modelled as turbulent heat exchange with the ambient warmer air at $T = 25\ ^{\circ}\mathrm{C}$. The turbulence is modelled in terms of an eddy viscosity dynamically calculated by means of the Smagorinsky formulation (i.e., an eddy viscosity is directly associated with the size of a mesh).

We chose a simple triangular domain to reproduce a cross-section of the natural lake: 50 m depth, 5,000 m long and length of slope 2,400 m with aspect ratio 0.02. Modelling was performed on a numerical grid: 100×30 cells (50×50 m), 50 layers (1 m each) in the vertical, time step of integration 2 s, no wind forcing with heating modelled as turbulent heat exchange with warmer air ($T = 10\ ^{\circ}\mathrm{C}$) and solar heating corresponding to the spring period at mid-latitudes (200 $\mathrm{Wt/m^2}$) with day–night variations. Wind forcing can significantly influence the thermal bar propagation in real lakes (Malm 1995; Rao *et al.* 2004) and thus must be taken into account, along with other particular conditions such as real bathymetry, bed resistance, wind friction, etc., when simulating real field cases. Here, we demonstrate only the principal physical situation, so it is not necessary to use any specific wind data.

The 12 passive tracers placed in the numerical domain revealed specific features of the subsurface jet propagation (four tracers were released from the points with coordinates (0.3, 0.3, −0.06), (0.43, 0.3, −0.06), (0.53, 0.3, −0.06), (0.83, 0.3, −0.06)) and downslope cascade propagation (four tracers were released from the points with coordinates (0.3, 0.3, −0.4), (0.43, 0.3, −0.06), (0.53, 0.3, −0.72), (0.83, 0.3, −0.94)). Special attention was paid to the intermediate onshore flow evolution (four tracers were released from the point with coordinates (0.3, 0.3, −0.14), (0.43, 0.3, −0.16), (0.53, 0.3, −0.22), (0.83, 0.3, −0.24)). Flow rates were calculated for positive flows only, over the entire water depth in the numerical basins, on the scale of the laboratory flume and lake for five and six locations, respectively, during the 3.98 °C-isotherm propagation.

RESULTS

PIV records of the thermal bar development

A deeper insight into the thermal bar as a complex phenomenon, containing downslope cascades, a subsurface jet and onshore flow in the intermediate layer (Demchenko 2007; Chubarenko *et al.* 2008), can be provided by the Particle Image Velocimetry (PIV) method: video records of the water flow, seeded with Pliolite particles, were taken and are described below.

At the beginning of the experiment, when the temperature everywhere is below T_m (Figure 2(a)), the entire basin is prone to vertical thermo-gravitational convection and the horizontal exchange between the shallow and deep parts is initiated by the downslope cascades. The maximum observed speed in this phase amounted to 0.6–0.7 mm/s. The downslope cascades' elevated leading edges are well pronounced: the velocity vectors are not parallel to the sloping bottom. When the water temperature is slightly higher than T_m at the top of the incline (Figure 2(b)), the speed of

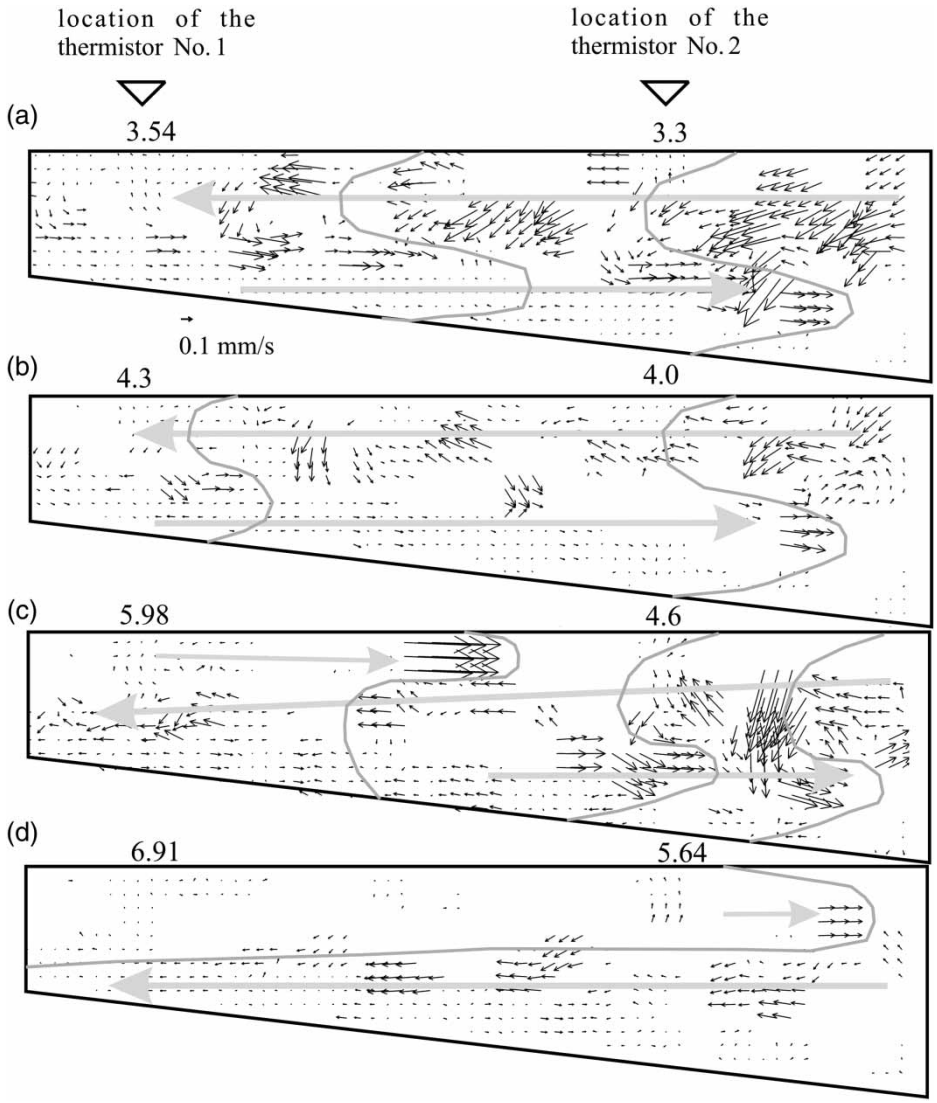

Figure 2 | Velocity vector maps in the middle part of the tank (x-axis = 0.48 m; z-axis = 0.075 m), from destabilising to stabilising buoyancy flux passing T_m at: (a) 40, (b) 65, (c) 80, (d) 105 s from the beginning of the experiment. The heat flux is roughly constant during the experiment. The values above every panel indicate surface temperature.

the downslope cascades is two times slower than at the beginning of the experiment (Figure 2(a)), at about 0.3–0.32 mm/s. While advancing the T_m, destabilising buoyancy flux decreases; however, the downslope cascades are still observed over the middle part of the slope.

When the temperature on thermistor No. 1 is already around 5.98 °C (Figure 2(c)), a subsurface jet (0.6 mm/s) is already evident over the middle of the slope and the downslope cascades are still observed in the deep part (the speed of particles there is about 0.55–0.6 mm/s). The horizontal temperature/density gradient between the top of the incline and the deep part quickly increases and the area of the maximum speed of the subsurface jet deepens. At the end of the domain, the downslope cascades completely disappear and a strong compensating flow (towards the shallow part of the basin) is observed in the intermediate layer (speed is around 0.2 mm/s) (Figure 2(d)).

It is important to note that the compensating flow permanently exists throughout the experiment. It provides the horizontal exchange at a depth varying around ~0.5H (where H = whole depth of the basin) between the shallow and deep parts, under both destabilising and stabilising buoyancy forcing.

Let us consider the variation with time of a buoyancy flux, $B = g\alpha F/c_p\rho$, m^2/s^3, where F is total heat flux, Wt/m^2, g is gravitational acceleration, m/s^2, $\alpha = 1/\rho(\partial\rho/\partial T)$ is thermal expansion coefficient of water, $^\circ C^{-1}$, c_p and ρ are thermal conductivity and density, respectively, at a given point of the tank (Figure 3). To calculate the buoyancy flux we use values of surface temperature, recorded by thermistor No. 1 during the experiment, and then define appropriate values of the thermal expansion coefficient. When the temperature is below T_m, the buoyancy flux due to heating from above is destabilising, which causes vertical mixing and the denser water to cascade downslope. Near T_m, the buoyancy flux becomes quite low, so the speed of the downslope cascades is two times slower than in the initial stage of the experiment. When passing T_m, the buoyancy flux sharply increases, being already a stabilising factor. The velocity field at this instant is characterised by a subsurface jet reaching the given point of the flume.

Numerical simulation results

Figure 4 reproduces numerical data for the time variation of the flow rate though one of the cross-sections in the numerical flow domain during the experiment. The flow rate in the positive (from the shore) direction is illustrated, which is integrated over the entire depth. At the beginning of the process, the intense downslope cascades propagate towards the deep part of the basin. After 30 min, they become weaker and flow rate decreases by 2.5 times. The warm subsurface jet and the 3.98 °C-isotherm reach the location of the given cross-section and the value of the flow rate gradually decreases. At the end of the experiment, the subsurface jet reaches the end of the numerical domain and the flow rate in the given cross-section drops to its minimum. It is important to note that the presence of the 3.98 °C-isotherm does not prevent the horizontal exchange between the shallow and deep parts of the basin, as was understood earlier. The flow rate decreases in the presence of the 3.98 °C-isotherm in the given cross-section but does not become zero.

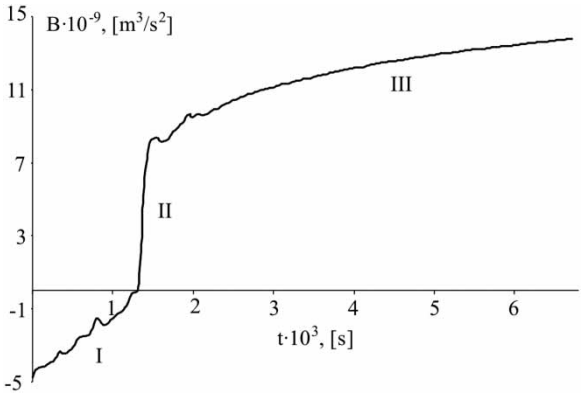

Figure 3 | Variation of the buoyancy flux through the surface B, m^3/s^2, with time t, at the location of thermistor No. 1, shown in Figure 2. Heat flux is nearly constant during the experiment. I – negative buoyancy flux, which is associated with the down-slope cascades; II – change of the sign of the buoyancy flux due to the passage through the 3.98 °C-isotherm; III – positive buoyancy flux, associated with the subsurface jet phase.

Numerical modelling results in the domain, reproducing a large deep lake, did show that, following the subsurface jet propagation over the whole length of the domain, there still remains a gravitationally unstable water mass with $T < T_m$ below the warm upper layer and there, the downslope cascades continue (see Figure 5). This is a striking feature in the dynamics of large deep water bodies (Baltic Sea, Lake Ladoga, Lake Onega, Lake Baikal), where the process of spring heating follows the same scenario: the upper layer is heated to temperatures $T > T_m$, while the deeper layers are still cooler. This means that the cold lake interior is involved in downslope cascading for a long time, even when the surface heating has resulted in an upper layer temperature $T > T_m$. The mechanism supporting a long-lasting vertical instability is the following: upper surface layer with temperatures $T > T_m$ is heated from above by solar radiation and is cooled below due to the existence of the cold interior; hence, this layer is stably stratified. Water with temperatures $T < T_m$ is heated from above because of the upper warm layer and vertical mixing is generated by thermo-gravitational convection (water temperature of the upper boundary of the cold core increases but is still below T_m; in accordance with the equation of state for fresh water, density value gradually increases). The thickness of the upper warm layer extends upwards with time; therefore, this mechanism will work until the cold core of the deep lake warms above T_m. The downslope cascading may be the reason for the occurrence of deep-water intrusions reported in Lake Baikal by Wüest *et al.* (2005). However, deep-water intrusions are much more complicated phenomena, with thermobaricity (combined effect of pressure and temperature on density, which reduces T_m at greater depths) playing an important role.

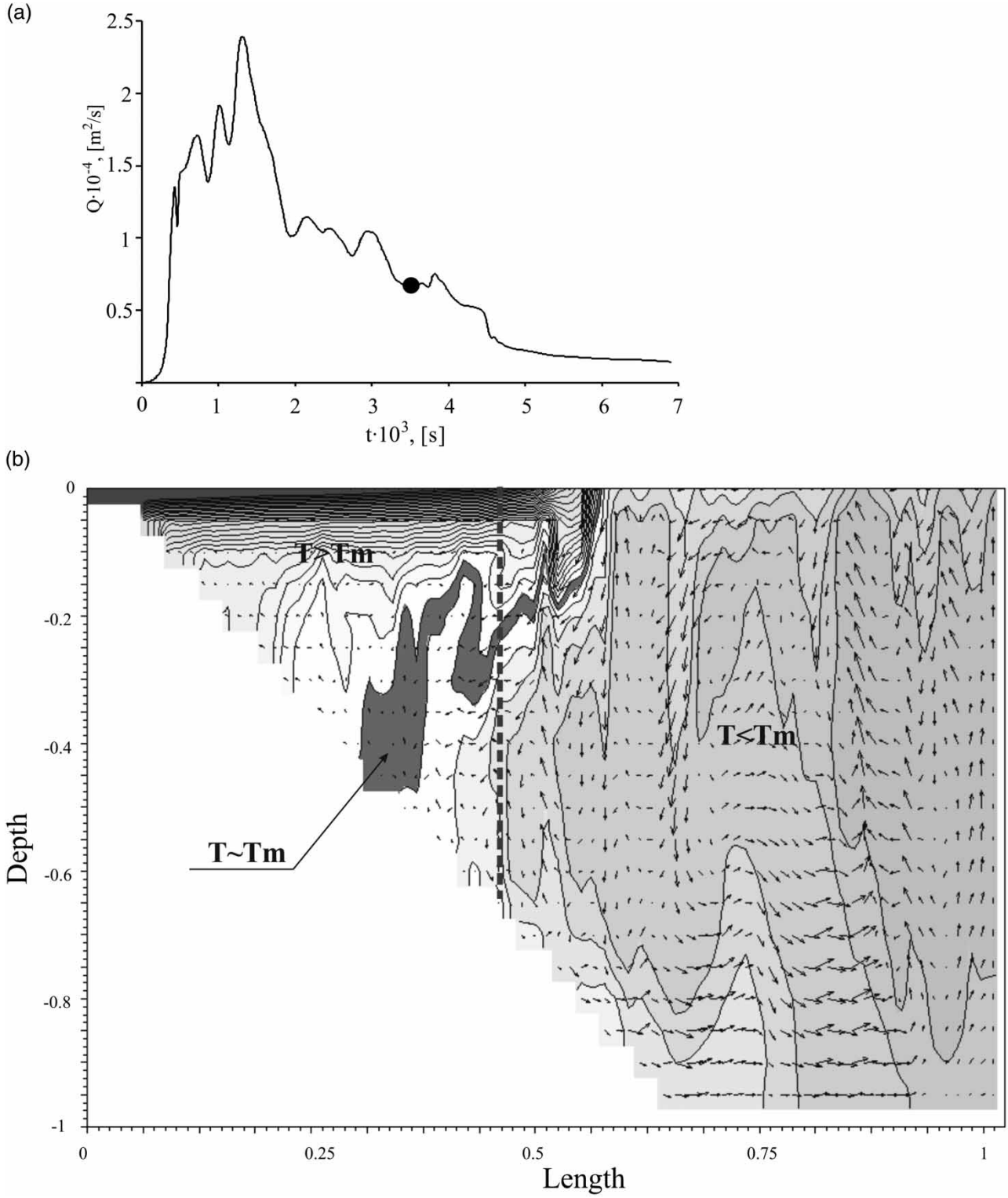

Figure 4 | (a) Flow rate variation in the given cross-section at the middle of the slope during the numerical experiment – the black circle marks the time instant when water temperature is around T_m in the given cross-section. (b) Graphical representation of numerical simulation results at the scale of laboratory flume: vertical cross-section at $t = 56$ min of simulated temperature and velocity fields for surface heating of an initially homogeneous fluid layer with a temperature $T = 0.5\ ^{\circ}C$. Isotherms are plotted for intervals of $0.058\ ^{\circ}C$ and are omitted above $5\ ^{\circ}C$ (in the upper layer). The velocity vectors clearly indicate the vertical convection due to a negative buoyancy flux from above in the entire region with temperatures $T < T_m$. The largest velocities are of the order of 1 mm/s.

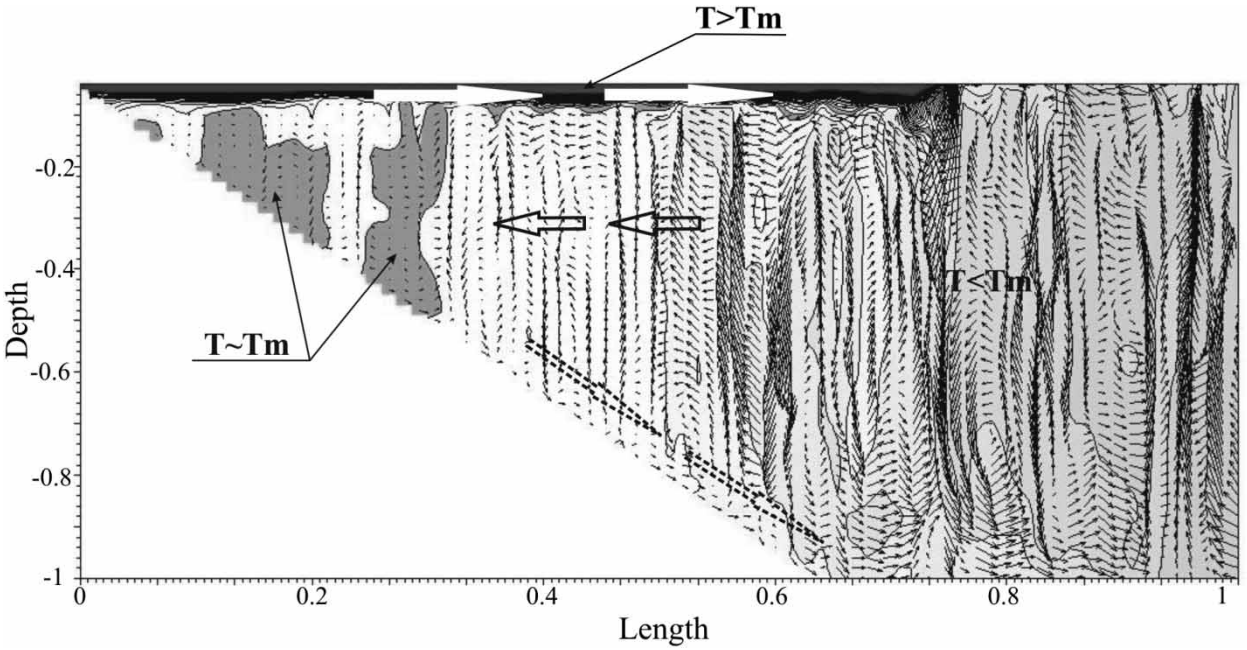

Figure 5 | Vertical cross-section of simulated temperature and velocity fields for heating from the surface of an initially homogeneous layer from $T = 0.5\ ^{\circ}C$. Isotherms are plotted every 0.058 °C and are omitted above 5 °C (in the uppermost layer). Velocity vectors show vertical convection due to negative buoyancy flux from above in the entire region with $T < T_m$, including waters below the warm surface jet. The largest velocities are of the order of 2–3 cm/s. Heating is modelled as turbulent heat exchange with warmer air and solar heating, corresponding to spring period at mid-latitudes with day–night variations and no wind.

Laboratory vs. numerical modelling results

The main goal of the previous work by Demchenko *et al.* (2012) devoted to the thermal bar phenomenon, was to reveal that the location of the convergence zone of the subsurface currents (when formed) does not coincide with that of the T_m-isotherm, as was asserted by Farrow (1995a, b) on the basis of numerical modelling results.

The evolution of the thermally driven flow seen in numerical simulations is very similar to that observed in laboratory experiments (Demchenko *et al.* 2012). During the surface heating, the water temperature over the slope reaches the critical value $T_m = 3.98\ ^{\circ}C$ and the less dense subsurface jet propagates towards the deep part, while the downslope bottom cascades are still observed in the deeper parts of the tank. Intense vertical mixing characterises the deeper part of the domain. A sketch of the flow structure in the presence of the T_m-isotherm, obtained from laboratory modelling, is in very good agreement with the numerical simulation results (see Figure 6). A remarkable feature shown is the evident formation and propagation of a compensating onshore flow in the intermediate layer. It is important for the present study to compare the various aspects of the flow and heat transfer processes in a more quantitative way, i.e., the temporal variations of the horizontal surface temperature gradients, density gradients and the speed of the subsurface jet.

The temporal variations of the horizontal surface temperature and density gradients, as measured by the five fixed thermistors in the presence of the 'spring' thermal bar in the 2-metre-long laboratory basin, was compared with the numerical simulation results (Demchenko *et al.* 2012). Generally, the horizontal temperature and density gradients in the stably stratified region are 3–8 and 20–50 times higher, respectively, than those in the unstably stratified region for the laboratory experiments. The horizontal temperature and density gradients in the stably stratified region are 3–13.5 and 7–40 times larger, respectively, than in the unstably stratified region for the numerical results, which is in good agreement with the experimental results.

We have also compared the speed of the 3.98 °C-isotherm propagation, which was obtained using two different grids, laboratory experiments of the 'spring' thermal bar in the 2-metre-long tank and the experimental results of Kreiman

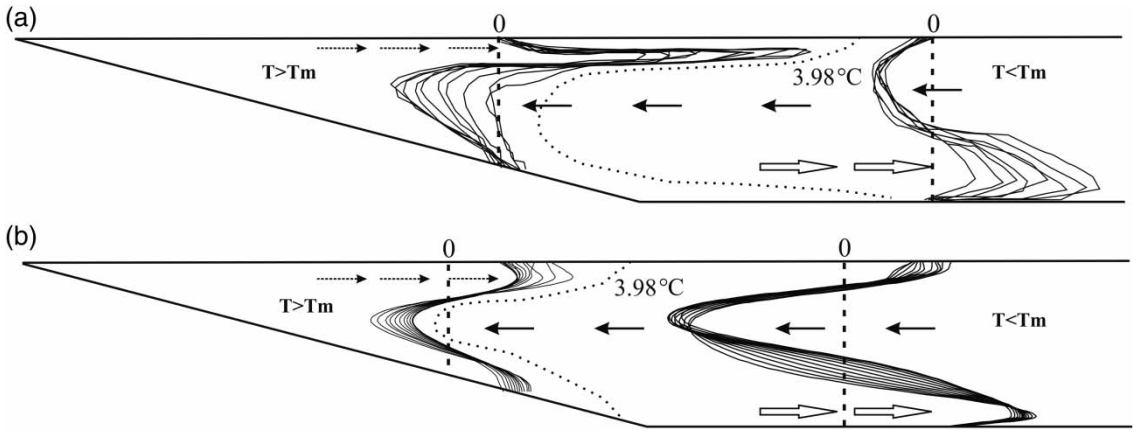

Figure 6 | Sketch of the flow structure in the presence of T_m in the laboratory tank, in the 'fast' stage of the thermal bar propagation based on (a) laboratory experiments (deformation of dye lines; from Chubarenko *et al.* (2008)); (b) numerical modelling results (isolines of the *u*-component of the horizontal velocity, grid (b)). Schematic arrows indicate the existence of the subsurface jet, intermediate onshore flow and downslope cascades in the laboratory experiments (Chubarenko *et al.* 2008) and also the numerical simulations.

(1989). In the numerical simulations, the run with a finer grid (320×80 cells) gave a speed of advancement of the 3.98 °C-isotherm in the 'slow' stage that is a factor of 1.2 times larger than in the run with the coarser grid (80×20 cells). However, in the 'fast' stage, the results for both runs are similar. For the laboratory results and numerical experiments, it was found that the distance x from the shore to the location of the 3.98 °C-isotherm at the free surface in the 'slow' stage depends on time as $x \sim t^{0.7-0.9}$, while in the 'fast' stage, the position develops as $x \sim t^{1.4-1.7}$, which is rather close to $x \sim t$ and $x \sim t^{1.5}$, respectively, as reported by Kreiman (Demchenko *et al.* 2012). Thus, the numerical simulations are in good agreement with the results of the laboratory experiments.

Experiments with tracers

We have performed an analysis of the concentration distribution of 12 passive tracers added in the upper layer, at the half-depth and near the bottom, for different locations and different time steps during thermal bar numerical modelling on the scale of lakes. We present a detailed analysis for the behaviour of one tracer (placed at (0.3, 0.3, −0.06) coordinate).

At the beginning of the 'fast' stage of the thermal bar propagation, the concentration of the passive tracer distributes over the whole depth (Figure 7(a)). Over time, a higher concentration is observed along the slope and in the area where the water temperature is very close to T_m over the whole depth (see Figures 7(b) and 7(c)). By the middle of the modelling, the higher concentration comes at the break point of the incline; it also propagates towards the very top of the incline, through the region where the water temperature is close to T_m (Figure 7(d)). At the final phase of thermal bar propagation, the higher concentration propagates towards the deep part of the tank in the surface layer, while it is still observable near the bottom. In the deep regions, where the water temperature is still below T_m, the higher concentration indicates the vertical convective mixing process (Figures 7(e) and 7(f)). The remarkable feature is the distribution of the higher concentration over the entire region, where water temperature is near T_m (Figures 7(a)–(f), empty dashed triangle).

The tracer experiment allows us to conclude that before reaching T_m, strong downslope cascades exist in the flow domain, and after reaching T_m at the top of the incline, a warm subsurface jet propagates towards the deep part of the domain. Onshore flow in the intermediate layer propagates to the top of the incline, through the water area with the temperature close to T_m. It is important to note that the horizontal water exchange intensifies between the shallow and deep parts, rather than restricting it in the presence of T_m; strong convective mixing, initiated by the downslope cascades, is still observed below the warm surface layer with the temperature higher than T_m.

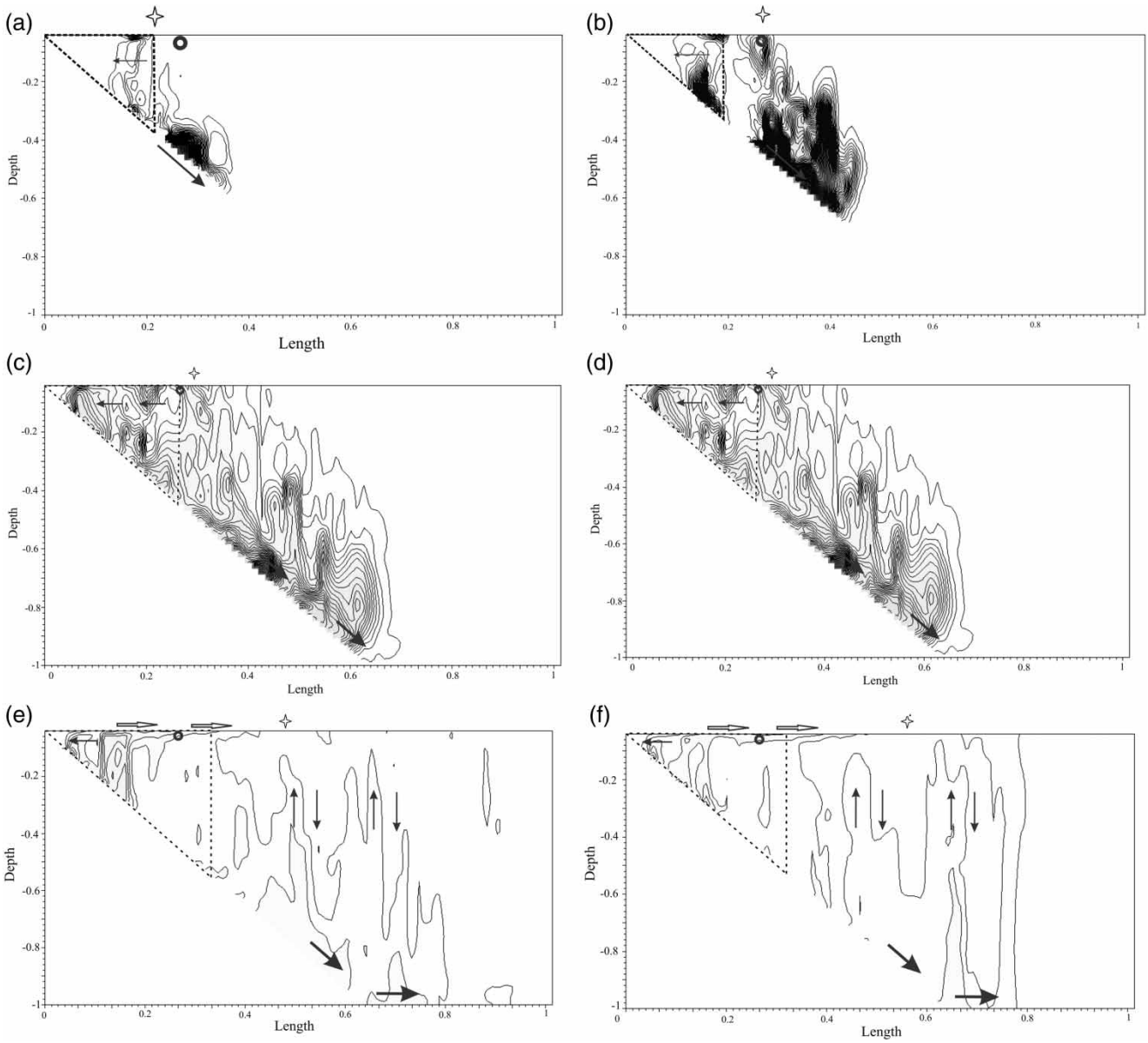

Figure 7 | Snapshots of consecutive concentration distributions of a passive tracer released from the point with coordinates (0.3, 0.3, −0.06) during the 'fast' stage of propagation of the thermal bar. An empty circle marks the point where the component was released, black arrows indicate the tracer propagation along the sloping bottom (cascades) and in the intermediate layers (compensating flow), empty arrows mark the upper layer (subsurface jet), vertical arrows mark thermo-gravitational convection in the deep parts; a star marks the T_m-isotherm position in the upper layer. The empty dashed triangle indicates the region where the water temperature is very close to T_m over the whole depth.

DISCUSSION

Numerical modelling allows us to estimate flow rates at different locations of the numerical domain on the scale of laboratory tanks and lakes during the 'fast' stage of the thermal bar progression. The velocity profiles, obtained from laboratory experiments, may be recalculated into flow rates. Moreover, using the speed of the horizontal flow and the thickness of the upper thermo-active layer, the flow rates can be expressed in dimensionless form using scaling analysis.

The main goal of this section is to obtain a dimensionless relationship linking the flow rate in a given cross-section with the thickness of the upper thermo-active layer.

First, we should explain our choice for the inertial scale rather than the viscous scale, which was used by previous investigators (Imberger 1974; Patterson & Imberger 1980; Bejan *et al*. 1981). We should estimate the order of inertial and viscous terms in the Navier–Stokes equation based on the results of laboratory experiments. For typical values we have: $\Delta\rho/\rho_0 \sim 10^{-5}$ kg/m^3, $h \sim 10^{-2}$ to 10^{-1} m, $g = 10$ m/s^2, $U \sim 10^{-4}$ m/s, $\nu \sim 10^{-6}$ m^2/s, $L =$ length of the tank $= 2$ m. Hence, the inertial term $[\Delta\rho/\rho_0 \times g \times h]$ is of the order of 10^{-6} to 10^{-5}; the viscous term $[\nu U/L^2]$ is of the order of 10^{-10}. Thus, we can conclude that inertia plays a key role in the propagation of the thermal bar.

Let U be a typical measure of the horizontal flow speed, L is horizontal length scale, e.g., distance from the very top of the incline to the location of T_m at the surface, increasing with time, h is typical vertical length scale, e.g., the thickness of the upper thermo-active layer (this is a layer where water temperature is higher than T_m over entire depth) and $\Delta\rho = (\rho_0 - \rho_1)$ is the characteristic horizontal density difference from the very top of the incline to the location of T_m at the surface, where ρ_0 is maximum density, ρ_1 is water density at the very top of the incline decreasing with time (see also Chubarenko 2010; Demchenko *et al*. 2012). Assuming that the horizontal flow is driven by a horizontal pressure gradient and governed by a balance between the inertial and pressure terms in the Navier–Stokes equation, one obtains for the scales:

$$U^2/L \sim 1/\rho_0 \times (g \times \Delta\rho \times h/L) \tag{1}$$

This gives for the horizontal velocity scale:

$$U \sim [g \times \Delta\rho/\rho_0 \times h]^{1/2} \tag{2}$$

where g and ρ_0 are the acceleration due to gravity and the reference density, respectively.

Taking into account the geometry, we can analyse the dependency on the bottom slope. Indeed, if the heating reaches depth h, then the horizontal distance S, from the shore to its location, $S = h/\mathrm{tg}\ \alpha$, is smaller near steeper slopes and larger for the gentle slopes. Thus, under the same heating conditions, the thermal bar propagation is faster near gentle slopes, which are, in addition, significantly more productive; hence, the values of the flow rates are much bigger. This conclusion is in full accordance with field observations (Naumenko & Karetnikov 1993).

To verify this formula for characteristic scales, we combined information regarding the propagation speed of the thermal bar on scales ranging from laboratory experiments to field observations in lakes. We used the results of laboratory experiments on 'spring' thermal bar modelling in a 2-metre-long tank (Demchenko *et al*. 2012), the experiments of Kreiman (1989), the experiments on 'spring' thermal bar modelling in a 5-metre-long tank (Chubarenko *et al*. 2008), the field measurements of Korosov *et al*. (2006) in Lake Ladoga, those of Mortimer (2004) in Lake Michigan and those of Rao *et al*. (2004) in Lake Ontario. The propagation speed U of the T_m-isotherm is very well approximated by (2): the best linear fit of the field, laboratory and numerical data is described by $y = 0.49x - 0.82$ (with $x = \log\ (h \times \rho/\rho_0)$ and $y = \log\ U$), with quite a high correlation coefficient, $R^2 = 0.88$ (Demchenko *et al*. 2012).

Thus, for the flow rate we have:

$$Q \sim U \cdot h \sim [g \times \Delta\rho/\rho_0]^{1/2} h^{3/2} \text{ or } Q = K[g \times \Delta\rho/\rho_0]^{1/2} h^{3/2} \tag{3}$$

where K is coefficient of proportionality of this relationship and will be found below.

To verify this relationship, it is useful to summarise the information about flow rates during the thermal bar development at different scales, ranging from laboratory experiments to numerical results on the scale of a lake. Figure 8 summarises the above-described numerical modelling results, obtained for the scales of the flume and a lake and the laboratory experiments reported in Chubarenko *et al*. (2008).

These data sets, presented in Table 1, cover spatial scales from centimetres to tens of metres. The solid line in Figure 8 is the best linear fit of the laboratory and numerical data, with quite a high correlation coefficient ($R^2 = 0.97$) and described by $y = 1.0x - 0.9$ (with $x = \log\ [(\Delta\rho/\rho_0)^{1/2}\ h^{3/2}]$ and $y = \log\ Q$). Evidently, the flow rates during the thermal bar evolution are well approximated by:

$$Q = 0.1[(g \times \Delta\rho/\rho_0)^{1/2} h^{3/2}] \tag{4}$$

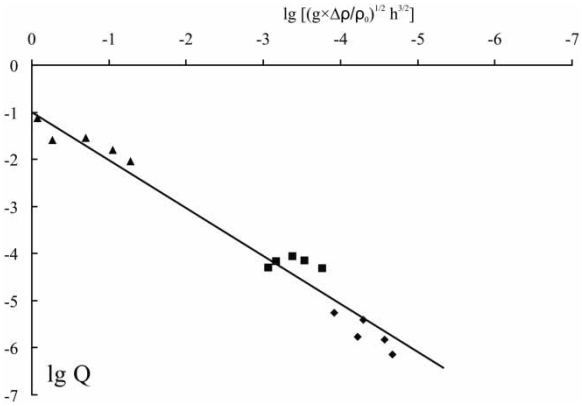

Figure 8 | The flow rates during the travel of the 3.98 °C-isotherm, Q [m^2/s], versus thickness of the thermo-active layer, h [m] and the horizontal density difference, $\Delta\rho/\rho_0$ [kg/m^3] determined from laboratory and numerical data. Symbols represent data from the laboratory experiment (Chubarenko *et al.* 2008): marked by ◆; the described numerical modelling results: ■ (scale of the flume) and ▲ (scale of a lake).

Overall, the high reliability of the linear approximation of the data corroborates that the flow rates during the thermal bar process depend on the vertical spatial scale and the relative density difference across the front.

The most exciting feature of the current field in the presence of T_m, which was obtained from the laboratory experiments, is the location of the maximum of the warm jet speed in the subsurface layer. Indeed, if the jet was the only result of the upper surface layer inclination due to the thermal expansion coefficient, the area where the maximum speed is observed must be at the surface and the speed of the subsurface jet must be some orders less. However, Chubarenko *et al.* (2007) showed that for various shapes of vertical temperature profiles, formed above the sloping bottom by stabilising buoyancy flux, the maximum of the horizontal pressure gradient is located at a depth of about $0.4d$ (there, d is the e-folding depth of the light penetration in a deep basin). This pressure gradient forces the intermediate water layer to move towards the shallows and displace the heated littoral waters. Thus, an internal pressure field rather than the surface inclination generates the motion of the surface layer and the velocity profile takes the shape of a convective exchange flow (see, for example, Mullarney *et al.* 2004). The velocity profile tends to become more or less symmetric relative to the half-depth level, so that in the deep area the upper half moves offshore, while the lower half moves onshore. The flow velocities are rather low, so that it happens even though the upper surface is stress-free, while there is friction at the bottom.

Based on the laboratory and numerical results, we will try to explain the field data results obtained by Rao *et al.* (2004) in Lake Ontario. At the beginning of the heating process, there is vertical convective mixing, which causes strong downslope cascades and a compensating onshore flow in the intermediate layer in the pre-thermal bar period, as was noticed by Rao *et al.* (2004). When water temperature reaches T_m at the surface, the value of the buoyancy flux is around zero (see Figure 3), which means a decrease in the speed of the downslope cascades (this is called the 'slow' phase of the thermal bar development (Elliot & Elliot 1970; Kreiman 1989)). The jet of warm water begins to form at the very top of the incline because of the appearance of the weak horizontal density gradient. This may push the waters forward and this impulse is transferred into the cold region, which leads to the occurrence of weak offshore surface currents far ahead of the 3.98 °C-isotherm, as was reported in Demchenko *et al.* (2012). This is in good agreement with field measurements in Lake Ontario. However, at the scale of a large lake, the buoyancy flux value is still very small during a rather long period. Hence, the thermal bar front may be stationary for up to several days or even weeks, as was observed by Rao *et al.* (2004). With further progressive heating, shallow water temperatures rise above T_m, so that the horizontal pressure (density) gradients quickly increase; the sign of buoyancy flux becomes positive and its value increases. The warm subsurface jet propagates towards the deep part of the basin over the mid-depths. With the increase of the thermally active layer thickness, the subsurface jet accelerates due to both progressive heat advection from shallows and heating from above. Therefore, the onshore compensating flow at intermediate depths is reinforced. Thus, the thermal bar in the 'fast' stage of its development intensifies rather than restricts the horizontal heat exchange between the shallow and the deep parts and this is in accordance with the field observations of Rao *et al.* (2004).

CONCLUSIONS

1. Laboratory and numerical experiments showed that during the entire process of thermal bar propagation, the compensating onshore flow is present at intermediate depths. Its intensity depends on the phase of the thermal bar development. Before reaching the 3.98 °C-isotherm, the onshore flow is very intense due to the negative buoyancy flux values. In the 'slow' stage of the thermal bar development, which is associated with the approach of the buoyancy flux to zero, the speed of the downslope cascades decreases considerably. In the 'fast' stage of the 3.98 °C-isotherm propagation, it is more intense due to larger buoyancy fluxes and stronger advection from the shallows. Thus, the thermal bar propagation in the 'fast' stage of its development supports horizontal transport.
2. The analysis of the concentration distribution of the passive tracers in the numerical basin at the scale of a lake presented a clear description of the flow field and showed that the compensating flow in the intermediate layers is observed during the thermal bar development and propagates onshore though the water area with the temperature very close to T_m.
3. The flow rate of the horizontal transport during the thermal bar propagation is a very important characteristic of the flow field. We attempted to link the flow rate to the spatial scale and horizontal density differences and this resulted in the relationship $Q = 0.1 \cdot [\Delta\rho/\rho_0^{1/2}\ h^{3/2}]$ with a correlation coefficient of $R^2 = 0.97$. This law provides an opportunity to estimate the value of flow rate, which may help to solve water pollution problems, appearing during the evolution of the 'spring' thermal bar, in the nearshore zone of large freshwater lakes.

ACKNOWLEDGEMENTS

This work was supported by INTAS YSF 06-1000014-6508, RFBR No. 10-05-00472a, 10-05-00540a. The authors would like to express great thanks to Prof. GertJan van Heijst for the opportunity to perform the laboratory experiments and also to Elke van Loenhout, Paul Bloemen and Ad Holten (Fluid Dynamics Laboratory, Eindhoven, The Netherlands) for the preparation of the experiments and technical assistance.

REFERENCES

Bejan, A., Al-Homound, A. & Imberger, J. 1981 Experimental study of high Rayleigh number convection in a horizontal cavity with different end temperatures. *J. Fluid. Mech.* **109**, 283–299.

Chubarenko, I. P. 2010 Horizontal convective water exchange above a sloping bottom: the mechanism of its formation and an analysis of its development. *Oceanology* **50**, 166–174.

Chubarenko, I. P., Afon, V. V. & Demchenko, N. Yu. 2007 On the hypothesis of convective formation of summer coastal up-welling. In: *Physical Problems of Ecology (Environmental Physics)* (V. I. Trykhin, Yu. A. Pirogov & K. N. Pokazeev, eds). MAKS Press, Moscow, Russia, pp. 402–410.

Chubarenko, I. P. & Demchenko, N. Yu. 2008 Laboratory modeling of the structure of the thermal bar and related circulation in a basin with a sloping bottom. *Oceanology* **48**, 327–339.

Demchenko, N. Yu. 2007 On the speed of subsurface jet propagation in presence of the temperature of maximum density: laboratory experiments. *Publs. Inst. Geophys. Pol. Acad. Sci.* **E-7** (401), 81–86.

Demchenko, N. Yu., Chubarenko, I. P. & van Heijst, G. 2012 On the fine structure of the thermal bar front. *Environ. Fluid. Mech.* **12** (2), 161–183.

Elliot, G. H. 1970 A mathematical study of the thermal bar. *Proc. of the 13th Conf. Great Lakes Res.*, pp. 545–554.

Elliot, G. H. & Elliot, J. A. 1970 Laboratory studies on the thermal bar. *Proc. of the 13th Conf. of Great Lakes Res.*, Ann Arbor, pp. 413–418.

Farrow, D. E. 1995a An asymptotic model for the hydrodynamics of the thermal bar. *J. Fluid. Mech.* **289**, 129–140.

Farrow, D. E. 1995b A numerical model for the hydrodynamics of the thermal bar. *J. Fluid. Mech.* **303**, 279–295.

Forel, F. A. 1901 Etudes thermiques des lacs du nord de 1'Europe. *Arch. Sci. Phys. Nat.* **12**, 35–55.

Gbah, M. B. & Murthy, C. R. 1998 Characteristics of turbulent cross and alongshore momentum exchanges during a thermal bar episode in Lake Ontario. *Nord. Hydrol.* **29**, 57–72.

Imberger, J. 1974 Natural convection in a shallow cavity with differentially heated end walls. Part 3. Experimental results. *J. Fluid. Mech.* **65**, 247–260.

Ivey, G. W. & Hamblin, P. F. 1989 Convection near the temperature of maximum density for high Rayleigh number, low aspect ratio, rectangular cavities. *Trans. ASME J. Heat Transfer* **111**, 100–105.

Korosov, A. A., Pozdnyakov, D. V., Filatov, N. N., Grassl, H., Mazourov, A. A., Loupyan, E. A. & Ionov, V. V. 2006 A satellite data-based study of seasonal and spatial variations of some ecoparameters in Lake Ladoga. *Earth Invest. Space* **5**, 76–85.

Kreiman, K. D. 1989 Thermal bar based on laboratory experiments. *Oceanology* **29**, 935–938.

Malm, J. 1995 Spring circulation associated with the thermal bar in large temperate lakes. *Nord. Hydrol.* **26**, 331–358.

Malm, J., Grahn, L., Mironov, D. & Terzhevik, A. 1993 Field investigation of the thermal bar in Lake Ladoga, spring 1991. *Nord. Hydrol.* **24**, 339–358.

Mortimer, J. 2004 *Lake Michigan in Motion*. University of Wisconsin Press, Madison, WI, USA.

Mullarney, J. C., Griffiths, R. W. & Hughes, G. O. 2004 Convection driven by differential heating at a horizontal boundary. *J. Fluid. Mech.* **516**, 181–209.

Naumenko, M. A. & Karetnikov, S. G. 1993 Application of the infrared satellite images for the study of the Ladoga Lake thermal regime. *Earth Invest. Space* **4**, 69–78.

Patterson, J. & Imberger, J. 1980 Unsteady natural convection in a rectangular cavity. *J. Fluid. Mech.* **100**, 65–86.

Rao, Y. R., Skafel, M. G. & Charlton, M. N. 2004 Circulation and turbulent exchange. *Limnol. Oceanogr.* **49**, 2190–2200.

Rodgers, G. K. 1966 The thermal bar in Ontario, spring 1965 and winter 1965–1966. *Proc. of 9th Conf. Great Lakes Res.*, University of Michigan, pp. 369–374.

Rymiantsev, V. A. & Drabkova, V. G. 2002 *Ladoga Lake: Past, Present and Future*. Nauka, Saint Petersburg, Russia.

Tikhomirov, A. I. 1982 *The Thermal Properties of Large Lakes*. Nauka, Leningrad, Russia.

Wüest, A. J., Ravens, T. M., Granin, N. G., Kocsis, O., Schurter, M. & Sturm, M. 2005 Cold intrusions in Lake Baikal: direct observational evidence for deep-water renewal. *Limnol. Oceanogr.* **50**, 184–196.

First received 11 November 2011; accepted in revised form 21 October 2012